

On the physical requirements for a pre-reionization origin of the unresolved near-infrared background

K. Helgason,¹★ M. Ricotti,² A. Kashlinsky^{3,4} and V. Bromm⁵

¹Max Planck Institute for Astrophysics, Karl-Schwarzschild-Str. 1, D-85748 Garching, Germany

²Department of Astronomy, University of Maryland, College Park, MD 20742, USA

³Observational Cosmology Laboratory, Code 665, NASA Goddard Space Flight Center, Greenbelt, MD 20771, USA

⁴SSAI, Lanham, MD 20706, USA

⁵Department of Astronomy, University of Texas, Austin, TX 78712, USA

Accepted 2015 September 22. Received 2015 September 15; in original form 2015 May 19

ABSTRACT

The study of the cosmic near-infrared background (CIB) light after subtraction of resolved sources can push the limits of current observations and yield information on galaxies and quasars in the early universe. Spatial fluctuations of the CIB exhibit a clustering excess at angular scales $\sim 1^\circ$ whose origin has not been conclusively identified, but disentangling the relative contribution from low- and high-redshift sources is not trivial. We explore the likelihood that this signal is dominated by emission from galaxies and accreting black holes (BHs) in the early Universe. We find that, the measured fluctuation signal is too large to be produced by galaxies at redshifts $z > 8$, which only contribute $\sim 0.01\text{--}0.05 \text{ nW m}^{-2} \text{ sr}^{-1}$ to the CIB. Additionally, if the first small mass galaxies have a normal initial mass function, the light of their ageing stars (fossils) integrated over cosmic time contributes a comparable amount to the CIB as their pre-reionization progenitors. In order to produce the observed level of CIB fluctuation without violating constraints from galaxy counts and the electron optical depth of the IGM, minihaloes at $z > 12$ must form preferably top-heavy stars with efficiency $f_* \gtrsim 0.1$ and at the same time maintain a very low escape fraction of ionizing radiation, $f_{\text{esc}} < 0.1$ per cent. If instead the CIB fluctuations are produced by high- z BHs, one requires vigorous accretion in the early universe reaching $\rho_{\text{acc}} \gtrsim 10^5 \text{ M}_\odot \text{ Mpc}^{-3}$ by $z \simeq 10$. This growth must stop by $z \sim 6$ and be significantly obscured not to overproduce the soft cosmic X-ray background and its observed coherence with the CIB. We therefore find the range of suitable high- z explanations to be narrow, but could possibly be widened by including additional physics and evolution at those epochs.

Key words: dark ages, reionization, first stars – diffuse radiation – early universe – galaxies: high-redshift.

1 INTRODUCTION

The cosmic near-infrared background (CIB) contains radiation that has been built up throughout the cosmic history, including highly redshifted emission from the pre-reionization era (see e.g. review by Kashlinsky 2005). Measured brightness fluctuations in deep source-subtracted CIB maps have established the existence of an unresolved CIB component in addition to resolved point sources (Kashlinsky et al. 2005, 2007a; Thompson et al. 2007a,b; Matsumoto et al. 2011; Kashlinsky et al. 2012; Cooray et al. 2012b; Seo et al. 2015). Whereas the CIB flux associated with this component cannot be directly determined from such measurements, the required levels

are nevertheless theoretically deduced (Kashlinsky et al. 2005) to lie well below earlier studies claiming high CIB (Dwek & Arendt 1998; Matsumoto et al. 2005; Tsumura et al. 2013; Matsumoto et al. 2015) in excess of integrated galaxy counts (Madau & Pozzetti 2000; Fazio et al. 2004; Keenan et al. 2010; Ashby et al. 2013), and at the same time consistent with indirect measurements from γ -ray blazars (Mazin & Raue 2007; Meyer et al. 2012; Ackermann et al. 2012; H.E.S.S. Collaboration 2013; Biteau & Williams 2015).

The unresolved CIB fluctuations measured with *Spitzer*/IRAC (Kashlinsky et al. 2005, 2007a, 2012; Cooray et al. 2012b), *Hubble Space Telescope* (*HST*)/NICMOS (Thompson et al. 2007a,b) and *AKARI*/IRC (Matsumoto et al. 2011; Seo et al. 2015), confirm a mutually consistent isotropic signal above the noise extending out to $\sim 1^\circ$ scales. The observed properties can be listed as follows (see Kashlinsky et al. 2015 for detailed discussion): (1) the signal is

*E-mail: kari@mpa-garching.mpg.de

inconsistent with local foregrounds such as the Zodiacal Light and Galactic cirrus (Kashlinsky et al. 2005; Arendt et al. 2010; Matsumoto et al. 2011; Kashlinsky et al. 2012). Its extragalactic nature is further supported by its isotropy (now measured in several different parts of the sky; Kashlinsky et al. 2012); (2) the signal is also inconsistent with the contribution from known galaxy populations at $z < 6$ extrapolated to faint luminosities (Helgason, Ricotti & Kashlinsky 2012); (3) the amplitude of the fluctuations increases towards shorter wavelengths showing a blue spectrum (Matsumoto et al. 2011; Seo et al. 2015); (4) there is no evidence yet for the fluctuations correlating significantly with the mask or the outer parts of removed sources (Kashlinsky et al. 2005; Arendt et al. 2010); (5) the large-scale clustering component does not yet appear to start decreasing as the small-scale shot noise power is lowered; (6) the clustering component of the fluctuations shows no correlation with faint *HST*/ACS source maps down to $m_{\text{AB}} \sim 28$ (Kashlinsky et al. 2007c); (7) the unresolved CIB fluctuations at $3.6 \mu\text{m}$ are coherent with the cosmic far-infrared background (200, 350, 500 μm) which can largely be explained by unresolved galaxies at low- z and their extended emission (Thacker et al. 2015); (8) the source-subtracted CIB fluctuations are coherent with the unresolved soft cosmic X-ray background (CXB; not detected in harder X-ray bands of $> 2 \text{ keV}$; Cappelluti et al. 2013) which can partly be accounted for by unresolved AGN and X-ray galaxies at low- z (Helgason et al. 2014). A recent measurement by Zemcov et al. (2014) finds the blue spectrum continuing to shorter wavelengths but appears to be in conflict with earlier *HST*/NICMOS and 2MASS fluctuation studies at the same wavelengths from 2MASS (Kashlinsky et al. 2002) and *HST*/NICMOS (Thompson et al. 2007a).

It was suggested that the era of the first stars could have left a measurable imprint in the CIB, both its mean level (Santos, Bromm & Kamionkowski 2002) and its anisotropies (Cooray et al. 2004; Kashlinsky et al. 2004). This was followed by more detailed studies on the nature of these populations (Salvaterra et al. 2006; Salvaterra & Ferrara 2006; Fernandez & Komatsu 2006; Kashlinsky et al. 2007b; Fernandez et al. 2010). This was motivated by the expectation that the first objects were (i) individually bright with a short epoch of energy release, (ii) highly biased as they form out of rare density peaks and (iii) radiate strongly in UV/blue being redshifted into today's near-IR part of the spectrum (reviewed in Bromm 2013). Despite being consistent with all observed properties however, the high- z origin of the source-subtracted CIB signal continues to be debated. This is in part because of the lack of a robust redshift determination of the signal and because recent models of early galaxy populations $z \gtrsim 6$ have failed to produce sufficient CIB fluctuation power (Fernandez et al. 2012; Cooray et al. 2012a; Yue et al. 2013a). This has motivated alternative hypotheses for their origin, such as in a diffuse intrahalo light at low-/intermediate- z (Cooray et al. 2012b; Zemcov et al. 2014). At the same time, it was suggested that accretion by direct collapse black holes (DCBH) at high- z can provide an explanation which also fully accounts for the CIB \times CXB signal (Yue et al. 2013b).

We evaluate the physical requirements for a pre-reionization origin of the CIB fluctuations based on the latest observational insights. We carefully quantify the clustering excess in Section 2. In Section 3, we use an analytic approach to model the CIB contributions from early stellar populations, both metal free and metal enriched. In Section 4, we consider accreting black holes (BHs) and associated gaseous emission. We derive the required star formation and accretion rates and discuss their implications for the CXB. In this paper, we use the standard Λ cold dark matter (Λ CDM) cosmology with parameters $(h, \Omega_m, \Omega_\Lambda, n_s, \sigma_8) = (0.678, 0.308, 0.692, 0.968,$

0.829) (Planck Collaboration XVI et al. 2014). All magnitudes are in the AB system (Oke & Gunn 1983).

2 QUANTIFYING THE CIB FLUCTUATION EXCESS

Brightness fluctuations in the CIB can be written $\delta F(\mathbf{x}) = F(\mathbf{x}) - \langle F \rangle$ where $F(\mathbf{x})$ is the sky brightness at the 2D coordinate \mathbf{x} and $\langle F \rangle$ is the mean isotropic flux. We describe the fluctuation field in terms of the power spectrum as a function of the angular wavenumber q , defined as $P(q) = \langle |\delta_q|^2 \rangle$, where δ_q is the 2D Fourier transform of the CIB fluctuation field, $\delta F(\mathbf{x})$. On the angular scale $\theta = 2\pi/q$, the root-mean-square (rms) fluctuation in the CIB can be written as, $\delta F_\theta \equiv \langle \delta F^2(\mathbf{x}) \rangle^{1/2} \simeq [q^2 P(q)/2\pi]^{1/2}$. The fluctuations are therefore determined by the flux of the underlying sources and how they cluster on the sky

$$\delta F_\theta = F_{\text{CIB}} \Delta_\theta, \quad (1)$$

where the information on the clustering as a function of angular scale is contained within the fractional fluctuations Δ_θ . At high- z , the sources trace increasingly rare peaks in the density field and Δ_{cl} can become $\simeq 0.1$ at arcminute scales. Current fluctuation measurements exhibit a signal above the noise which flattens to an approximately constant rms value towards large angular scales (see Fig. 1). In this paper, we refer to the *clustering* as the average of this large-scale value $\Delta_{\text{cl}} \equiv \langle \Delta(3\text{--}30 \text{ arcmin}) \rangle$. When defining our CIB fluctuation excess, we focus on NIR fluctuations at $2 < \lambda < 5 \mu\text{m}$ from *AKARI*/IRC and *Spitzer*/IRAC. This is where current measurements show a mutually consistent large-scale signal which at the same time are deep enough such that the clustering component is not sensitive to further decreasing the shot noise from remaining galaxies.

In order to get a single representative value for the measured large-scale CIB fluctuations from high- z , we consider a simple three-parameter model consisting of the sum of fluctuations from unresolved galaxy populations at the measurement detection threshold (Helgason et al. 2012) and Λ CDM power spectrum¹ (Eisenstein & Hu 1998), projected to $z = 10$:

$$\delta F_\theta^2(\lambda) = a \cdot \delta F_{\Lambda\text{CDM}}^2 \left(\frac{\lambda}{3.6 \mu\text{m}} \right)^{-2b} + c_i \cdot \delta F_{\text{gal}}^2(\lambda). \quad (2)$$

We explore the parameter space by least-squares fitting the available data from *AKARI* and *Spitzer* (at 1–50 arcmin) in 10^6 Markov-Chain Monte Carlo steps. We use Metropolis–Hasting acceptance with chain burn-in of 10^5 steps and priors on the parameters $-1 < \log a < 1$, $-3 < \log b < 3$, $-2 < \log c < 5$. As each measurement has different source detection threshold we allow the last term in the above equation to vary at each measurement depth such that c_i is a free parameter in six different measurements (making the effective number of parameters eight). For the first term, we obtain $a = 1.79_{-0.41}^{+0.38}$ and $b = 1.77_{-0.51}^{+0.68}$. We display the 68 per cent confidence regions of the best fit in Fig. 1 for which we obtain $\chi^2/\text{dof} = 1.62$. The quality of the fit is limited by the slight disagreement in the data of Cooray et al. (2012b) versus Kashlinsky et al. (2012), particularly at $4.5 \mu\text{m}$ where our single power-law spectral slope favours the latter. It is worth noting that the best-fitting excess fluctuation signal, $\sim \lambda^{-1.8}$, does not exhibit a Rayleigh–Jeans type spectrum, $\sim \lambda^{-3}$ as indicated by measurements of the net large-scale

¹ The power spectrum is normalized at the 10 arcmin peak such that $\delta F_{3.6 \mu\text{m}} = 0.043 \text{ nW m}^{-2} \text{ sr}^{-1}$.

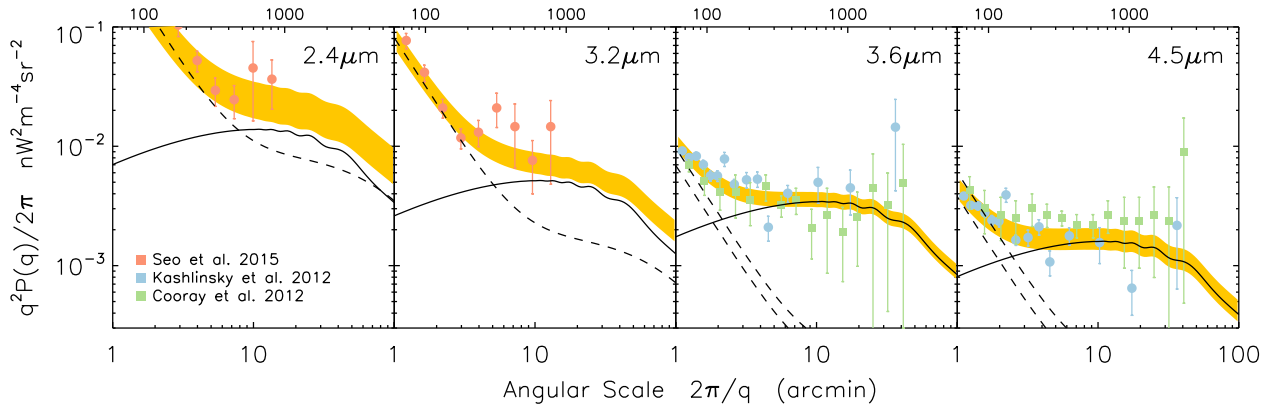


Figure 1. The latest measurements of the mean-square CIB fluctuations in the 2–5 μm range. *AKARI*/IRC measurements are shown as red circles (Seo et al. 2015) whereas *Spitzer*/IRAC are shown in blue circles (Kashlinsky et al. 2012) and green squares (Cooray et al. 2012b). The solid curve shows the best-fitting Λ CDM power spectrum projected from $z = 50$ to $z = 10$ whereas the dashed lines correspond to the unresolved galaxy populations from Helgason et al. (2012) fitted to each individual measurement (see text). The fit gives $\chi^2/\text{dof} = 1.62$. The upper horizontal axis shows the angular scale in arcseconds. The large-scale-averaged fluctuations in each band are $\delta F((3\text{--}30 \text{ arcmin})) = (0.11, 0.068, 0.056, 0.037)_{-(0.037, 0.012, 0.006, 0.009)}^{+(0.044, 0.013, 0.006, 0.01)}$ $\text{nW m}^{-2} \text{sr}^{-1}$ at (2.4, 3.2, 3.6, 4.5) μm .

signal. The reason is the contribution of remaining low- z galaxies: (1) because the abundance of low- z galaxies is greater at the typical detection thresholds at $<2 \mu\text{m}$, i.e. their number counts are steeper, and (2) because experiments at smaller wavelengths happen to be shallower than those at $>2 \mu\text{m}$ such that less of the low- z galaxy contribution is removed. The Spectral Energy Distribution (SED) of the best-fitting excess can be seen in Fig. 6. Integrating the first term in equation (2) over 2–5 μm we obtain the excess fluctuation

$$\delta F_{\text{CIB}} = \left[\int_{2 \mu\text{m}}^{5 \mu\text{m}} \delta F^2 \frac{d\lambda}{\lambda} \right]^{1/2} = 0.072_{-0.020}^{+0.023} \text{ nW m}^{-2} \text{sr}^{-1}. \quad (3)$$

This compares well with the analytical estimate in Kashlinsky et al. (2015). We will refer to this value of $\delta F_{\text{CIB}} = 0.072 \text{ nW m}^{-2} \text{sr}^{-1}$ as our requirement for any high- z model to reproduce the data in Fig. 1. We also make our equations directly scalable with Δ_{cl} such that the associated CIB flux $F_{\text{CIB}} = \delta F_{\text{CIB}} \Delta_{\text{cl}}^{-1}$ can be easily compared with measurements of the isotropic CIB, both direct and those derived from TeV blazars.

At a given near-IR wavelength, the isotropic CIB flux is related to the comoving specific emissivity $j_\nu(z)$ per unit volume of the sources

$$F_{\text{CIB}} \equiv \int_{2 \mu\text{m}}^{5 \mu\text{m}} I_\lambda d\lambda = \frac{c}{4\pi} \iint j_\nu(z) \frac{dt}{dz} \frac{dv}{1+z}, \quad (4)$$

where $\nu = \nu_{\text{obs}}(1+z)$ is the rest-frame frequency. If the CIB was released during the first $\Delta t \simeq 500 \text{ Myr}$, it follows from this equation that the luminosity density $\rho_L \equiv \nu j_\nu$ at optical wavelengths $0.2 \lesssim \lambda_{\text{CIB}}/(1+z) \lesssim 0.5 \mu\text{m}$ must reach a representative value of (see also Kashlinsky et al. 2007b)

$$\rho_L = 1.5 \times 10^9 L_\odot \text{ Mpc}^{-3} \left(\frac{\Delta_{\text{cl}}}{0.1} \right)^{-1} \left(\frac{1+z}{10} \right) \left(\frac{\Delta t}{500 \text{ Myr}} \right)^{-1}, \quad (5)$$

where we have substituted $\Delta_{\text{cl}} = \delta F_{\text{CIB}}/F_{\text{CIB}}$. This luminosity density is notably higher than the output during the peak of star formation history at $z \sim 1\text{--}2$. If the CIB fluctuations originate at high- z , the luminosity density must have been substantially higher in the early universe regardless of the nature of the sources. In the following sections, we investigate the basic astrophysical requirements for both stellar and accretion powered emission.

3 STELLAR SOURCES

3.1 High- z galaxy populations

An increasing number of galaxies are being detected out to $z \sim 10$ as the deep Hubble program are being pushed to the limits of the instrument capabilities (Bouwens et al. 2007; McLure et al. 2009; Ellis et al. 2013; Finkelstein et al. 2015a; Bouwens et al. 2015). While these galaxies compose merely the tip of the iceberg at these redshifts, it is of interest to estimate the expected contributions of the entire population to the unresolved CIB. Here, we present a simple forward evolution model of the conditional luminosity function which we tune to fit observations at $z \sim 8\text{--}10$. We assume that galaxies form in haloes with a star formation rate (SFR) proportional to their collapse rate at z

$$\dot{\rho}_*(M, z) = f_* \frac{\Omega_b}{\Omega_M} \frac{d}{dt} M n(>M_{\text{min}}, t), \quad (6)$$

where f_* is the average fraction of baryons in collapsed haloes that are processed into stars and $n(M, t)$ is the evolving halo mass function, which we adopt from Tinker et al. (2008). In order for star formation to take place, haloes must reach a sufficient size, M_{min} , to shock heat the baryons to the virial temperature allowing for efficient gas cooling. The relation between the mass of a halo and its virial temperature is $M_{\text{min}} = 3 \times 10^6 M_\odot \left(\frac{T_{\text{vir}}}{2000 \text{ K}} \right)^{3/2} \left(\frac{1+z}{10} \right)^{-3/2}$, where we have assumed a mean molecular weight of 1.22 for neutral primordial gas composed of H and He. For the discussion of high- z galaxies, we will adopt the limit of $T_{\text{vir}} = 40 \text{ 000 K}$, somewhat higher than the threshold for cooling via atomic hydrogen. Star formation in smaller haloes will be addressed in the following subsection. Luminosity and spectra are assigned to star-forming galaxies using the *Yggdrasil* model, a population synthesis code designed to model high- z systems containing varying mixtures of PopII and III stars (Zackrisson et al. 2011). This model includes the nebular contribution from photoionized gas and extinction due to dust, with single age stellar population (SSP) taken from Leitherer et al. (1999, PopII) and Schaerer (2002, PopIII, with no mass loss). Because observed Lyman-break galaxies show no evidence of anything other than metal-enriched star formation, we adopt a universal Kroupa initial mass function (IMF; 0.1–100 M_\odot) with a metallicity of $Z = 0.0004$, characteristic of PopII stars (we call this IMF₁ in the

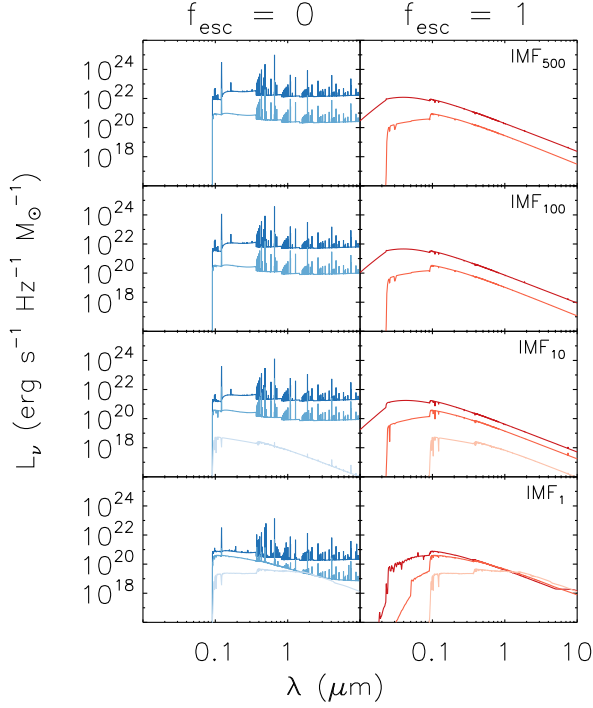


Figure 2. The single age stellar population spectra from the *Yggdrasil* code. The three rows show energy spectra for different metal-free/poor IMFs. From top to bottom panels: heavy IMF with characteristic mass $\sim 100 M_{\odot}$, intermediate IMF $\sim 10 M_{\odot}$ and metal-poor stars with a normal Kroupa IMF (see text for details). The left- and right-hand panels show the SSP spectra for the two limiting cases of $f_{\text{esc}} = 0$ and 1, respectively. The three curves in each of the panels show the single age population at 0 and 3.6 Myr (top two) and 0, 10, 100 Myr (bottom two).

discussion below and Fig. 2). The volume emissivity of haloes with masses between M and $M + dM$ at z is obtained by convolving the SSP with the star formation occurring prior to z

$$j_{\nu}(M, z) = \int_z^{\infty} \dot{\rho}_*(M, z') \mathcal{L}_{\nu}(t_z - t_{z'}) \frac{dt}{dz'} dz', \quad (7)$$

where $\mathcal{L}_{\nu}(t_{\text{age}})$ is the aging spectral template shown in Fig. 2. At any given epoch, each halo includes the instantaneous emission from newly formed stars as well as older populations from earlier episodes of star formation. The luminosity function is $\Phi(L)dL = \Phi(M)dM$ where the relation between mass and luminosity is $L(M) = \nu j_{\nu}(M, z)/(Mn(M, z))$. The CIB flux production history seen at frequency ν_{obs} as a function of halo mass is

$$f(M, z) = \frac{c}{4\pi} j_{\nu}(M, z) \frac{\nu}{1+z} \frac{dt}{dz}, \quad (8)$$

where j_{ν} is evaluated at $\nu = \nu_{\text{obs}}(1+z)$. The net CIB is then simply $F_{\text{CIB}} = \int f(M, z) dM dz$. This can be used to derive the angular power spectrum of CIB fluctuations via projection of the source clustering (Limber 1953)

$$P(q) = \int \frac{H(z)}{cd^2(z)} \left[\int f(M, z) b(M, z) dM \right]^2 P_3(qd^{-1}, z) dz, \quad (9)$$

where $H(z) = H_0 \sqrt{\Omega_M(1+z)^3 + \Omega_{\Lambda}}$ and $d(z)$ is the comoving distance. The clustering is described both in terms of the evolving matter power spectrum in 3D, $P_3(k, z)$ (Eisenstein & Hu 1998) and the mass-dependent halo bias, $b(M, z)$ (Sheth, Mo & Tormen 2001).

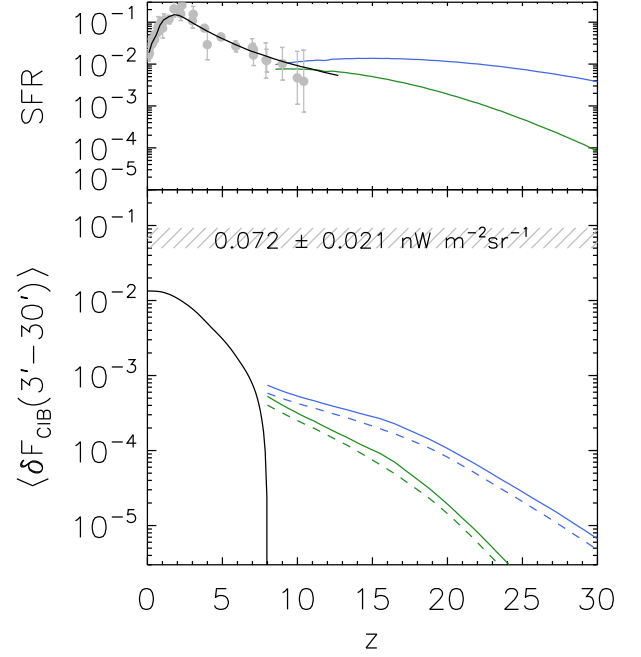


Figure 3. Upper: the SFR in haloes ($T_{\text{vir}} > 4 \times 10^4$ K, green) and mini-haloes ($T_{\text{vir}} > 10^3$ K, blue). The SFR data points, compiled in Robertson et al. (2015), are derived from the UV luminosity function integrated down to $0.001 L^*$. The solid line shows the maximum likelihood SFR history from the same work. These connect well with our modelled SFR at higher z assuming $f_* = 0.005$. Bottom: the build-up of large-scale-averaged CIB fluctuations from galaxies forming stars with IMF₁ and efficiency $f_* = 0.005$. The solid and dashed lines correspond to $f_{\text{esc}} = 0$ and 1, respectively. Fluctuations from low- z galaxy populations remaining after removing galaxies brighter than $m_{3.6\mu\text{m}} = 25$ are shown as the black solid line (Helgason et al. 2012). The reference level of the observed large-scale fluctuations is shown as the hatched region (grey).

In this description, the bias is coupled to the brightness distribution of haloes, eliminating the need for assumptions on the halo occupation number of galaxies. We also note that variations in the cosmological parameters, in particular σ_8 , affect the amplitude of the power spectrum and add uncertainty to our modelling. Equation (9) is equivalent to the two-halo term describing the correlation between central haloes² (Seljak 2000; Cooray & Sheth 2002).

The large-scale CIB fluctuations resulting from our modelled high- z galaxies are shown in Fig. 3. We have chosen a constant star formation efficiency (in both M and z) in such a way to obtain a good agreement with the observed star formation rate and UV Luminosity function (LF) at high- z . This value we find to be $f_* = 0.005$. Fig. 4, compares the relative abundance of high- z galaxies (green) with the source density of all $z < 8$ galaxies (blue). It is immediately clear that compared to current measurements, star-forming galaxies with a normal IMF are underdominant at least out to 32 mag and, with these assumptions, do not reach the measured fluctuation levels (see Fig. 3). This is true regardless of whether the LF is cut off at $M_{\text{UV}} \simeq -14$ mag or extrapolated to much fainter systems. Simply increasing f_* further would overproduce the LF at

² In this paper, we neglect the one-halo term from high- z sources since it is always negligible compared to the two-halo term at the relevant angular scales (> 3 arcmin).

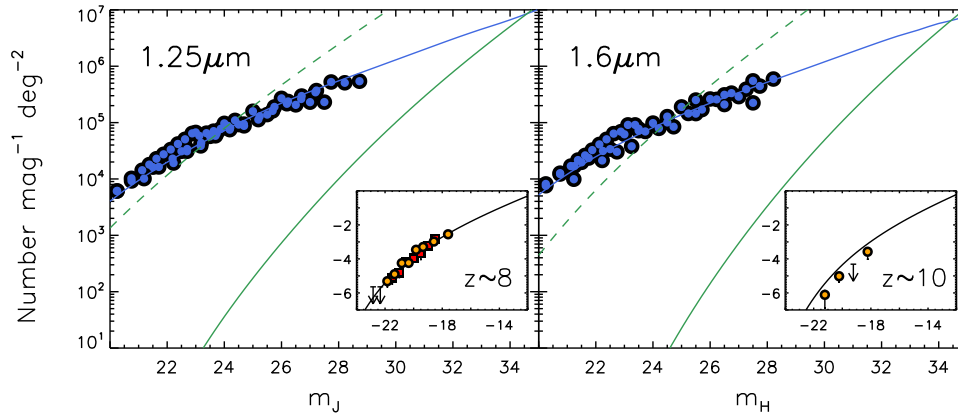


Figure 4. Deep source counts at 1.25 (left) and 1.6 μm (right). The blue data points represent galaxy counts, mostly from $z \sim 1\text{--}3$ at these deep magnitudes. The galaxy counts model of Helgason et al. (2012) is shown as blue solid line and extrapolated to faint magnitudes whereas the green line shows the counts for galaxies at high- z ($f_* = 0.5$ per cent, IMF_1), with the Lyman dropouts placing them at $z \gtrsim 8$ (left) and $z \gtrsim 10$ (right). The comparison of low- z and high- z counts suggests that the faint-end of the high- z galaxy population will only become significant at $\gtrsim 32$ mag. The dashed lines show the model that would be required to reproduce the CIB fluctuations, δF_{CIB} , at these redshifts. The fact that these models are in gross conflict with both the LF data and the deepest counts suggests that any such signal must either come from higher z or be confined in isolated minihaloes at the faint-end. The insets show the luminosity function $\log(\text{mag}^{-1} \text{Mpc}^{-3})$ versus M_{UV} of our default high- z galaxy model ($f_* = 0.5$ per cent, IMF_1 , $f_{\text{esc}} = 12$ per cent) tuned to fit measurements (Finkelstein et al. 2015a; Bouwens et al. 2015).

$z \sim 8\text{--}10$ and eventually also the faint NIR number counts (this was already pointed out by Salvaterra & Ferrara 2006). In fact, fluctuations from faint unresolved galaxies at low- z produce a larger signal than high- z galaxies. We therefore conclude, in agreement with Cooray et al. (2012a) and Yue et al. (2013a), that the measured CIB fluctuation levels cannot be reproduced by high- z galaxies with reasonable extrapolations of their evolving luminosity function.

3.2 Minihaloes and PopIII

There are two ways of having more light produced by stars without overproducing the observed LF at $z \sim 8\text{--}10$. First, that an epoch of more vigorous light production took place before $z \sim 8\text{--}10$; in other words, the era of CIB production already ended before this time. Secondly, the sources are outside the sensitivity limit of the deepest surveys, i.e. they are found in numerous isolated haloes that are intrinsically fainter than $M_{\text{AB}} \simeq -17$ mag. This would be exhibited in a rise in the faint-end of the LF, either by greater star formation efficiency in smaller haloes or by heavier IMF. However, numerical studies tend to show the opposite, that the efficiency decreases with lower masses (Ricotti, Gnedin & Shull 2002a,b, 2008; Behroozi, Wechsler & Conroy 2013; O’Shea et al. 2015). In this subsection, we relax the assumption of a constant $f_* = 0.005$ and $T_{\text{vir}} = 40\,000$ K and explore whether greater values can be accommodated where observational constraints are not yet available. In other words, what happens if we, in addition to high- z galaxies $\gtrsim 10^8 M_\odot$, include the contribution of the first stars forming out of pristine metal-free gas in minihaloes $\gtrsim 10^6 M_\odot$?

The IMF of the first PopIII stars is highly uncertain but is expected to be biased towards high masses (Bromm 2013). It is also unclear whether stars forming under H_2 -governed cooling (sometimes called PopIII.1) differ substantially from those forming in a second episode governed by atomic H line emission (PopIII.2). We therefore consider four different IMFs of the Yggdrasil model for stars forming in haloes down to the smallest minihaloes equivalent to the H_2 cooling threshold 1000 K.

- IMF₁: standard Kroupa in the 0.1–100 M_\odot range.*
- IMF₁₀: lognormal with characteristic mass of 10 M_\odot and dispersion of 1 M_\odot in the 1–500 M_\odot range.*
- IMF₁₀₀: power law $\propto M^{-2.35}$ in the 50–500 M_\odot range.*
- IMF₅₀₀: all stars are 500 M_\odot , near-Eddington.*

For details, we refer to Zackrisson et al. (2011) and references therein. Spectral evolution templates for these IMFs are shown in Fig. 2.

Fig. 5 shows the average star formation efficiency required to produce the measured $\delta F_{\text{CIB}} = 0.072 \text{ nW m}^{-2} \text{ sr}^{-1}$ at any given epoch for the three IMFs considered. It is clear that under these assumptions the CIB fluctuations can only be reproduced if minihaloes $\sim 10^6 M_\odot$ are allowed to continuously form massive stars with a high efficiencies $f_* > 0.1$. Furthermore, deep NIR counts limit this possibility to the most heavy IMFs where much of the energy output is reprocessed into nebular emission, $f_{\text{esc}} = 0$ (see also Fernandez et al. 2010). This is assuming that stars form continuously without mechanical or radiative feedback which is known to have strong impact on both f_* and f_{esc} (e.g. Jeon et al. 2014; Pawlik, Schaye & Dalla Vecchia 2015). In Fig. 6, we display the full CIB model with a simple description of chemical feedback which models the PopIII–PopII transition in terms of semi-analytic modelling of supernova (SN) winds (Furlanetto & Loeb 2005) which we adopt from Greif & Bromm (2006)

$$\dot{\rho}_{\text{PopIII}} = p_{\text{pris}}(z)\dot{\rho}_*, \quad (10)$$

where $\dot{\rho}_*$ is the net SFR from equation (6) and p_{pris} is the fraction of collapsed objects that are still chemically pristine. We display two cases of PopIII–PopII transition in Fig. 6, standard and delayed enrichment corresponding to $z_{1/2} = 11$ and 15, respectively, where we have defined $z_{1/2}$ as the redshift at which half of all star formation is in metal-enriched mode.³ The PopII assumes IMF_1 whereas we display the cases where PopIII takes on IMF_{10} , IMF_{100} and IMF_{500} .

³ The enrichment histories are modified by varying the radiation loss parameter $K_w^{1/3}$ (see Greif & Bromm 2006).

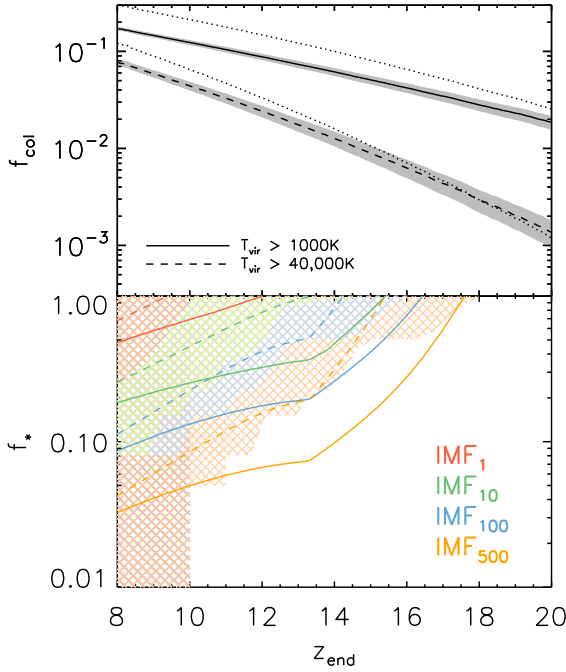


Figure 5. Upper: the fraction of mass in collapsed structures as a function of redshift. Solid and dashed lines correspond to haloes with $T_{\text{vir}} > 1000$ ($\gtrsim 10^6 M_{\odot}$) and $> 40\,000$ K ($\gtrsim 10^8 M_{\odot}$), respectively, for the Tinker et al. (2008) mass function. Dotted lines show the classic Press & Schechter (1974) prediction for comparison. The grey regions show the scatter associated with the 1σ uncertainties in the Planck cosmological parameters. Lower: the star formation efficiency f_* required to produce the reference level of the CIB fluctuations, δF_{CIB} , by a given redshift, z_{end} . The curves assume the entire stellar population forming with IMF₁, IMF₁₀, IMF₁₀₀, IMF₅₀₀ (red, green, blue, orange) in all haloes. The solid lines show the case where minihaloes $T_{\text{vir}} > 1000$ K are included whereas the dashed lines include $T_{\text{vir}} > 40\,000$ K haloes only. We have set $f_{\text{esc}} = 0$ in all cases and note energy requirements become even greater for $f_{\text{esc}} > 0$. The coloured regions show the combination of f_* and z_{end} that result in the overproduction of deep NIR counts data and/or LF data for the IMFs in the same colour scheme (see Fig. 4). These regions are thus forbidden unless the bright-end of the LF is suppressed, e.g. if f_* much lower in high-mass haloes than in low-mass ones.

Only the most extreme models ($f_* > 0.1, f_{\text{esc}} \ll 1, \text{IMF}_{100, 500}$) come close to the fluctuation excess shown in the right-hand panel as a grey region.

3.3 Ionizing photons

High star formation efficiencies coupled with a heavy IMF imply a vigorous production of ionizing photons (> 13.6 eV). These photons must either be absorbed locally by neutral gas within the halo, or escape and be absorbed by still neutral parts of the IGM. The injection rate of ionizing photons can be derived self-consistently from the SFR combined with the stellar population synthesis models at $z > 10$

$$\dot{n}_{\text{ion}}(z) = \int_{>13.6\text{eV}h^{-1}} \int \frac{j_{\nu}(M, z)}{h\nu} dM dv. \quad (11)$$

For the production of ionizing photons at later times $z < 10$, we adopt the prescription of Robertson et al. (2015) where \dot{n}_{ion} is derived from fitting the measured star formation rate history (see

Fig. 3). We calculate the ionization fraction of the IGM, x_{ion} , by solving

$$\dot{x}_{\text{ion}} = \frac{f_{\text{esc}} \dot{n}_{\text{ion}}(z)}{\langle n_{\text{H}} \rangle} - \frac{x_{\text{ion}}}{t_{\text{rec}}}, \quad (12)$$

where $\dot{n}_{\text{ion}}(z)$ is the production rate of intrinsic ionizing photons per comoving volume and $\langle n_{\text{H}} \rangle$ is the average comoving number density of hydrogen. The recombination time-scale is $t_{\text{rec}} = [C\alpha_B n_{\text{H}}(1 + Y/4X)(1 + z)^3]^{-1}$ where $C = \langle n_{\text{H}}^2 \rangle / \langle n_{\text{H}} \rangle^2$ is the clumping factor of ionized hydrogen, $\alpha_B(20\,000\text{ K})$ is the case-B recombination coefficient (Hummer 1994) and $X = 0.76$ and $Y = 1 - X$ are hydrogen and helium abundances. This allows us to derive the Thompson optical depth to the electron scattering

$$\tau_e = c\sigma_{\text{T}} \langle n_{\text{H}} \rangle \int x_{\text{ion}}(z) \left(1 + \frac{\eta Y}{4X}\right) (1 + z)^3 \frac{dt}{dz} dz, \quad (13)$$

where we assume helium is singly ionized at $z > 3$ ($\eta = 1$) and fully ionized at later times ($\eta = 2$). This can be compared with the latest values inferred from CMB polarization measurements from Planck $\tau_e = 0.066 \pm 0.012$ (Planck Collaboration XIII et al. 2015), which were found to be somewhat lower than earlier results from WMAP $\tau_e = 0.088 \pm 0.014$ (Hinshaw et al. 2013).

In Fig. 7 (left), we show the integrated optical depth to electron scattering, τ_e , as a function of redshift for our preferred IMF₁ model of high- z galaxies. Forcing the model to reproduce the latest Planck measurements requires $f_{\text{esc}} = 12$ and 5 per cent for minimum host halo mass corresponding to $40\,000$ ($\sim 10^8 M_{\odot}$) and 10^3 K ($\sim 10^6 M_{\odot}$), respectively. For the somewhat higher WMAP-derived τ_e these values are $f_{\text{esc}} = 32$ and 12 per cent, respectively. We caution that, since we did not include any feedback effects which tend to suppress the star formation efficiency at small host halo masses, the average escape fraction may be somewhat higher.

For a given SFR and IMF, the injection rate of ionizing photons into the IGM is simply proportional to f_* and inversely proportional to f_{esc} . Fig. 7 (right) shows the combination of f_* and f_{esc} that give a fixed $\tau_e = 0.066$ for our four IMFs. The figure shows that in order to maintain the required f_* and at the same time avoid reionizing the universe too early (and overproducing τ_e), one must maintain a very low average escape fraction $f_{\text{esc}} \lesssim 0.1$ per cent at $z > 10$. It follows that the $\gtrsim 99$ per cent of the ionizing photons need to be absorbed by the local gas which itself can only constitute $(1 - f_*) < 90$ per cent of the available baryons in these small haloes. Several studies modelling the propagation of ionization fronts within haloes hosting the first galaxies show that the escape fraction increases towards smaller mass (Ricotti & Shull 2000; Johnson et al. 2009). For star formation efficiencies $f_* > 10^{-3}$, Ferrara & Loeb (2013) find that ionizing photons escape very easily with $f_{\text{esc}} \simeq 1$ across a wide range of halo mass. Only the most massive haloes, $\gtrsim 10^8 M_{\odot}$ are able to confine their UV photons effectively. The escape fraction is also expected to increase towards higher redshifts making it hard to justify large f_* in high- z minihaloes (Kuhlen & Faucher-Giguère 2012; Mitra, Ferrara & Choudhury 2013). There are recent indications from determinations of the high- z LF that the star formation efficiency is actually increasing at early times (Finkelstein et al. 2015b). While it is not clear whether this trend extends to the lowest mass haloes where cooling relies on H_2 , observations of the stellar mass function in local dwarf systems suggest that small atomic cooling haloes at high- z could indeed be very efficient sites of star formation (Madau, Weisz & Conroy 2014).

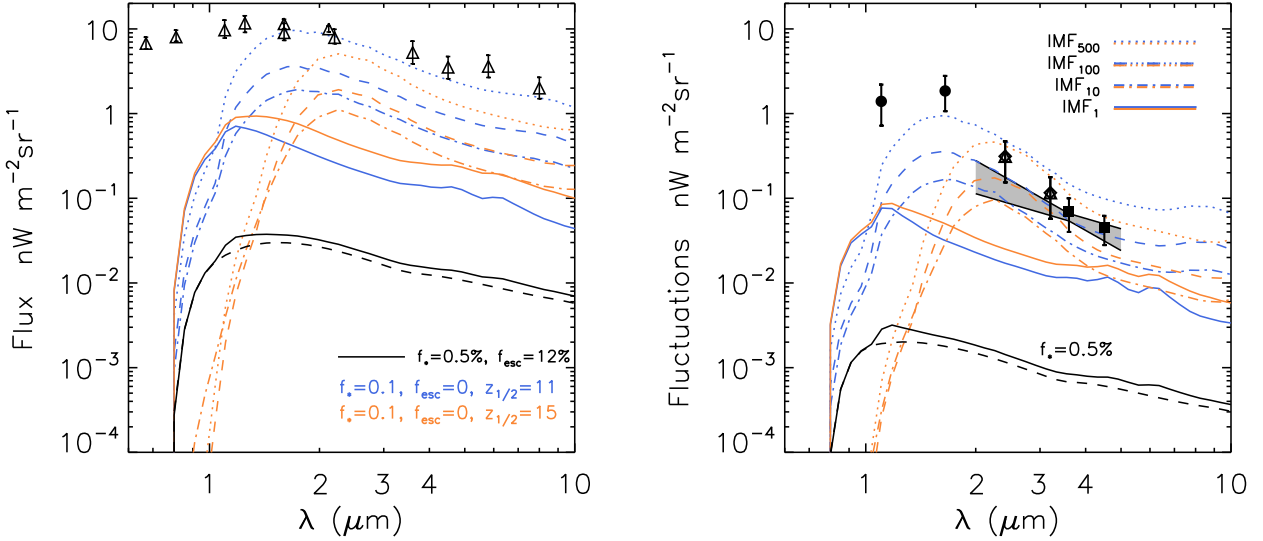


Figure 6. The spectrum of the CIB flux, $F_{\text{CIB}} = \nu I_\nu$ (left) and large-scale fluctuations, $\delta F_{\text{CIB}} = \sqrt{q^2 P / 2\pi}$ (right) for models of $z > 8$ early stellar emission. Fluctuations are averaged in the angular range 3–30 arcmin. The observationally motivated model of high- z galaxies, with $f_* = 0.005$ and IMF_1 is shown for $f_{\text{esc}} = 0.12$ (black solid line) and $f_{\text{esc}} = 1$ (black dashed) for comparison. The coloured set of lines correspond to models with $f_* = 0.1$, IMF_1 representing PopII (solid), and three cases of PopIII IMF_{10} , IMF_{100} , IMF_{500} (dot-dashed, dashed, dotted). The amplitude of both flux and fluctuations is directly scalable with f_* . Orange corresponds to a PopIII–PopII transition with $z_{1/2} = 15$ according to equation (10), whereas blue illustrates the case of a delayed enrichment with $z_{1/2} = 11$ (see text). All star formation is ended at $z = 8$. Models shown in blue and orange are for $f_{\text{esc}} = 0$ since $f_{\text{esc}} > 0.1$ per cent already violates reionization constraints explained in Section 3.3. Left: the data points is CIB from integrated galaxy counts which is naturally much greater than the high- z contribution. Right: the grey shaded region shows the best-fitting CIB fluctuation excess obtained in Section 2 after the contribution of low- z galaxies has been accounted for. The data in the right-hand panel are large-scale-averaged fluctuation measurements of Zemcov et al. (2014, filled circles), Matsumoto et al. (2011, open diamonds), Seo et al. (2015, filled diamonds) and Kashlinsky et al. (2012, filled squares). We do not show 2MASS and *HST*/NICMOS measurements as they do not reach sufficient angular scales for proper comparison at 3–30 arcmin.

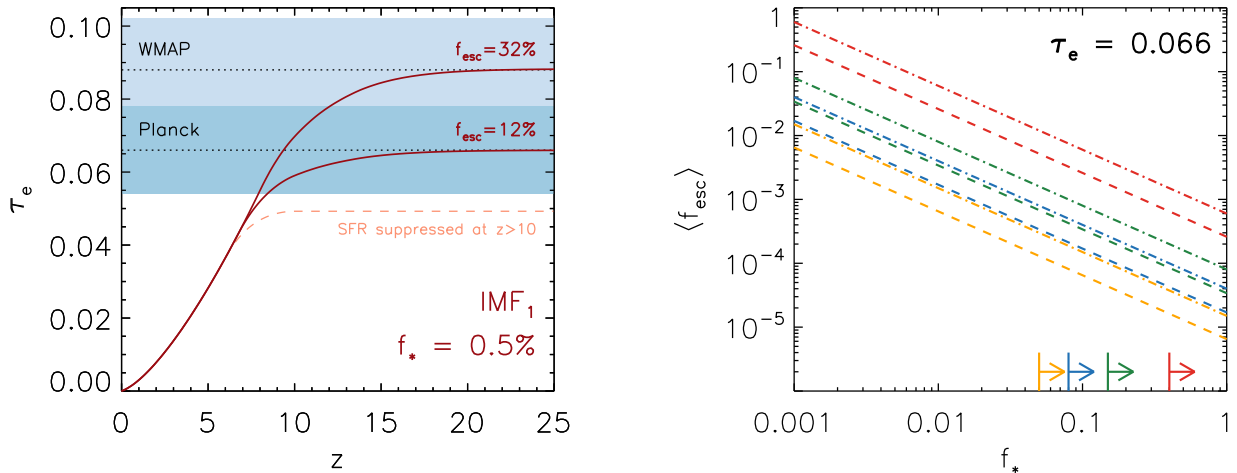


Figure 7. Left: the Thomson electron scattering optical depth integrated over redshift for our standard model of galaxy formation at $z > 10$. The $z < 10$ contribution shown in light red is derived from the measured star formation rate history shown in Fig. 3 (see Robertson et al. 2015). The red lines show the escape fraction tuned to match τ_e from Planck (lower) and *WMAP* (upper) which are indicated as horizontal dotted lines with blue regions showing the 1σ uncertainty. Right: the mean escape fraction versus star formation efficiency in all collapsed haloes for a fixed value of $\tau_e = 0.066$ assuming the four IMFs in the same colour scheme as in Fig. 5. Dashed corresponds to a cooling threshold of $T_{\text{vir}} > 1000$ K ($\sim 10^6 M_\odot$) and dot-dashed to $T_{\text{vir}} > 40000$ K ($\sim 10^8 M_\odot$). In order to reproduce δF_{CIB} and at the same time be consistent with reionization, the combination of $(f_{\text{esc}} f_*)$ must be concentrated in the lower right corner. The arrows denote the minimum required f_* are taken from Fig. 5 (lower) at $z = 10$.

3.4 Supernova contribution

The contribution of SN to the CIB was briefly discussed by Cooray & Yoshida (2004) who argued that SNe would remain subdominant with respect to the stellar contribution. The net energy radiated in a core-collapse SN is $E_{\text{SN}} \sim 10^{51}$ erg out of which only 0.1–1 per cent

emerges as electromagnetic radiation. For comparison, a star burning 10 per cent of its initial hydrogen emits $E_* = 10^{52} (M_*/M_\odot)$ erg over its lifetime, out of which only a fraction of this energy will end up in the CIB, depending on the spectrum and redshift. A crude calculation can be made based on our model by assuming that every $> 8 M_\odot$ star explodes as an SN for our three IMFs above. Even if

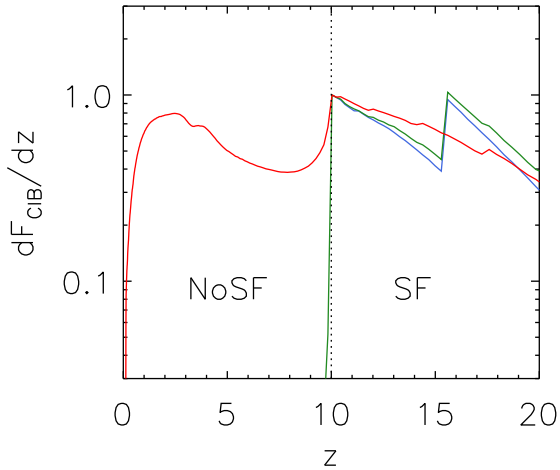


Figure 8. The integrated 2–5 μm flux production when star formation is turned off at $z = 10$, normalized to unity at $z = 10$ (arbitrary units). The red curve corresponds to a standard IMF_1 containing ageing low-mass stars in all $T_{\text{vir}} > 10^3 \text{ K}$ ($\gtrsim 10^6 M_{\odot}$) haloes. The green and blue lines show the heavier IMF_{10} and IMF_{100} , respectively, where the CIB contribution drops quickly after star formation is shut off as heavier stars die. The curves have been normalized at $z = 10$ for easier comparison.

every SN inputs a generous 10^{49} erg into the CIB, the contribution is always < 0.1 per cent of the stellar main-sequence contribution. It is therefore safe to ignore SNe as a major CIB contributor even in the case of some unusually bright SN types (pair-instability supernovae, hypernova) that have been proposed (Barkat, Rakavy & Sack 1967; Iwamoto et al. 1998).

3.5 Fossils of the first galaxies

Around the time of reionization, it is expected only systems with sufficient mass ($\gtrsim 10^8 - 10^9 M_{\odot}$) will be shielded from photoheating and continue to form stars. The majority of the already collapsed low-mass systems can nevertheless continue to contribute to the CIB through ageing stellar populations that continue to radiate throughout cosmic time. Locally, these systems are referred to as the fossils of the first galaxies (Ricotti & Gnedin 2005; Bovill & Ricotti 2009). These will not be as intrinsically bright as their high- z progenitors but can in principle accumulate substantial CIB by emitting at much lower z and for much longer span of time. Our formalism outlined above accounts for the ageing of populations and allows us to estimate the fossil contribution at later times. Approximating reionization as a step function, we turn off the SFR at $z = 10$ and allow the galaxies to passively evolve to $z = 0$. Not all fossil stars will contribute to the source-subtracted CIB as many systems will be incorporated into larger haloes hosting star-forming galaxies that are masked and subtracted in a fluctuation study (Bovill & Ricotti 2011a,b). For simplicity, we do not account for any subtraction of the fossil contribution and the calculation presented here includes all star-forming progenitors at $z > 10$. This should therefore be taken as an upper limit to the source-subtracted CIB for pre-reionization fossils. Note, however that this simple picture has recently been challenged by recent evidence showing that many dwarf systems continued to form stars even well after the universe was reionized (e.g. Weisz et al. 2014).

Fig. 8 shows the emission history of star-forming galaxies ($z > 10$) and their remnant fossils ($z < 10$). Shortly after SFR is set to zero, the flux from IMF_{10} and IMF_{100} drops quickly as

more massive stars die out but for IMF_1 the contribution of the remaining low-mass stars gradually rises towards lower z due to the $(1+z)^{-1}$ factor in equation (4). Interestingly, when integrated over redshift the CIB contribution from fossils is ~ 70 per cent of the net contribution whereas high- z galaxies make up only ~ 30 per cent. This suggests that the fossil contribution should be included in the net energetics of background radiation. However, considering that the low- z part is an *upper* limit for the fossil contribution, this is still insufficient to account for the measured δF_{CIB} . It will only become important if the corresponding high- z contribution is shown to be significant.

4 ACCRETION POWERED EMISSION

CIB originating from accretion on to BHs offers a more energetically favourable scenario due to the more efficient conversion of mass to energy. Such a scenario is particularly attractive for explaining the CIB in light of the observed coherence with the CXB (Capelluti et al. 2013) and the expectation that the progenitors of supermassive black holes (SMBHs) in the local universe were growing rapidly during this epoch (see Volonteri & Belloc 2012, for review). With an average radiative efficiency of accretion $\epsilon = L/\dot{M}c^2$, a BH will increase its mass by $\dot{M} = (1 - \epsilon(M, t))\dot{M}_{\text{in}}$ where \dot{M}_{in} is the net incoming mass accretion rate. Throughout this section, we will assume a constant efficiency, $\epsilon(M, t) = \text{const}$ with a caveat that relaxing this assumption may alter the numerology that follows. The net energy density radiated by a BH population can be related to mass density accreted before redshift z_{end} (Soltan 1982)

$$\rho_{\text{acc}}(z_{\text{end}}) = \frac{1 - \epsilon}{\epsilon c^2} \int_{z_{\text{end}}}^{\infty} \frac{dt}{dz} dz \int v j_v(z) dv \quad (14)$$

which is independent of the individual masses of the BH population. The energy output is related to the accretion rate via $\rho_L = \epsilon \rho_{\text{acc}} c^2$ for which the CIB can be written (see equation 4)

$$F_{\text{CIB}} = \frac{c^3}{4\pi} \int_{z_{\text{end}}}^{\infty} \epsilon \dot{\rho}_{\text{acc}} dt \int_{v_0}^{v_1} \frac{b_v dv}{1+z}, \quad (15)$$

where b_v is the average emerging spectrum, normalized such that $\int b_v dv = 1$ and taken to be independent of mass and time. When the last term is roughly constant or slowly varying at early times (in particular for a blue spectrum sloping up with shorter wavelengths) the net CIB from accretion processes is simply proportional to the net mass accreted by redshift z_{end} , i.e. $F_{\text{CIB}} \propto \rho_{\text{acc}}$. In other words, *with these assumptions the CIB is mostly independent of both the growth history and the individual masses of the BHs*. It follows from equations (1) and (15) that the accreted mass density required to produce the CIB fluctuations by redshift z_{end} is roughly

$$\rho_{\text{acc}} \simeq 2 \times 10^5 M_{\odot} \text{ Mpc}^{-3} \left(\frac{\delta F_{\text{CIB}}}{0.072 \text{ nW m}^{-2} \text{ sr}^{-1}} \right) \times \left(\frac{\Delta_{\text{cl}}}{0.2} \right)^{-1} \left(\frac{\epsilon}{0.1} \right)^{-1} \left(\frac{1+z}{10} \right) \left(\frac{f_{\text{sed}}}{1.0} \right)^{-1}, \quad (16)$$

where ϵ is the time-averaged efficiency, f_{sed} is a bolometric correction factor, i.e. the fraction of the total energy emitted that ends up being observed in the NIR (2–5 μm). This requirement is illustrated in Fig. 9. With maximal efficiency ($\epsilon = 0.4$) we require a minimum of $\rho_{\text{acc}} > 4 \times 10^4 M_{\odot} \text{ Mpc}^{-3}$ for producing the CIB fluctuations. If this is to be reached at high- z , any accretion activity by these BHs at later times would inevitably grow the net mass density locked in BHs further. Given the brief cosmic time elapsed at high- z , this lower limit for the accreted mass is quite large in comparison with

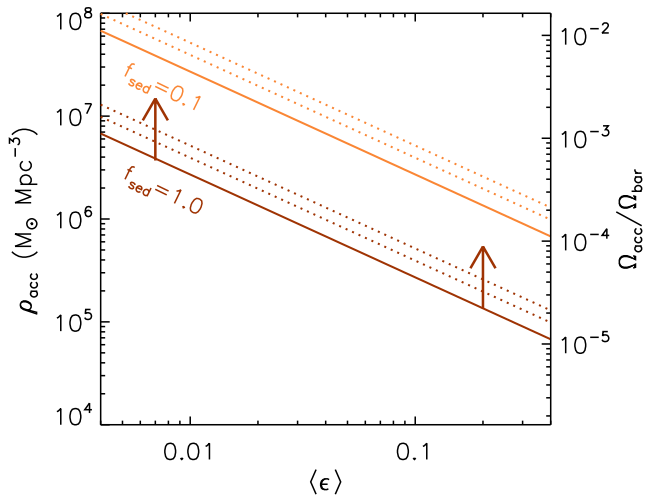


Figure 9. The requirements for accreted mass density and time-averaged efficiency to produce the reference δF_{CIB} level. The lower limit corresponds to $f_{\text{sed}} = 1$ when all the energy emitted ends up being observed in the NIR. The requirements increase quickly as the spectrum becomes broader $f_{\text{sed}} < 1$. The solid lines correspond to $z_{\text{end}} = 10$ whereas the dotted lines show $z_{\text{end}} = 15, 20$ (lower/upper). The right vertical axis shows the accreted density as a fraction of the baryonic density.

the mass density in SMBHs in the local universe $z = 0$, estimated at $(4 - 5) \times 10^5 M_{\odot} \text{Mpc}^{-3}$ (Shankar et al. 2004; Marconi et al. 2004; Vika et al. 2009).⁴ Other studies place additional limits on the mass density at $z \sim 6$ to $\lesssim 10^4 M_{\odot} \text{Mpc}^{-3}$ based on the unresolved CXB (Salvaterra et al. 2012); and $\lesssim 10^3 M_{\odot} \text{Mpc}^{-3}$ based on the integrated X-ray emission of high- z sources (Treister et al. 2013). Both these limits can however be avoided if the emerging SED is significantly altered, or if BH cores are heavily obscured or the accretion is radiatively inefficient. Relaxing the assumptions of constant ϵ would likewise alter these numbers. Nevertheless, for the CIB to be entirely from high- z we require an abundant radiatively efficient population of BHs established very early on, with significantly slowed/inefficient growth over the majority of the remaining cosmic time (see e.g. Tanaka, Perna & Haiman 2012). Whether the required ρ_{BH} is in fact realistically attainable is a matter of debate and outside the scope of this paper. In what follows we do not need to make assumptions on the BH seed masses and growth mechanism but will instead assume that the required ρ_{acc} can be reached by $z = 10$ and explore the observational consequences.

4.1 Correlation with the unresolved cosmic X-ray background

The recently detected cross-correlation signal between the unresolved CIB (3.6 and 4.5 μm) and CXB (0.5–2keV) fluctuations was suggested to originate from BHs in the early universe (Cappelluti et al. 2013). After accounting for unresolved AGN and X-ray binaries within galaxies, Helgason et al. (2014) find that a tentative CIB \times CXB signal (2.5σ) remains at large scales exhibiting the same shape as the CIB fluctuation power spectrum. From the definition of the spatial coherence $\mathcal{C}(q) = P_{\text{CIB} \times \text{CXB}}^2 / (P_{\text{CIB}} P_{\text{CXB}})$ and that $(\delta F^2) \simeq q^2 P(q) / 2\pi$ one can write

$$\delta F_{\text{CIB} \times \text{CXB}}^2 = \sqrt{\mathcal{C}} \delta F_{\text{CIB}} \delta F_{\text{CXB}}, \quad (17)$$

⁴ Recent evidence suggests this could be as much as five times higher than previously estimated (Comastri et al. 2015).

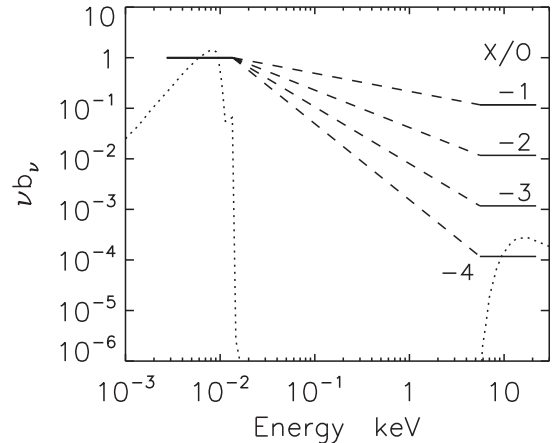


Figure 10. A simplistic broad-band SED in the rest frame with two contributions (1) optical/UV which is normalized to unity, and (2) a hard X-ray component which is a factor of $10^{-1}, 10^{-2}, 10^{-3}, 10^{-4}$ less energetic. For reference, the dotted curves show the emerging spectrum from the DCBH model of Yue et al. (2013b) also normalized to unity in the UV/optical. These spectra are used as templates in Fig. 11.

where $\delta F_{\text{CIB} \times \text{CXB}}$ is the CIB \times CXB cross rms-fluctuation. Taken at face value, the large-scale average (3–30 arcmin) of this measurement gives $\delta F_{\text{CIB} \times \text{CXB}} \sim 10^{-11} \text{erg s}^{-1} \text{cm}^{-2} \text{nW m}^{-2} \text{sr}^{-2}$. With the CIB fluctuations being roughly $\delta F_{4.5 \mu\text{m}} \simeq 0.04 \text{nW m}^{-2} \text{sr}^{-1}$ (see Section 2) we must have $\sqrt{\mathcal{C}} \delta F_{\text{CXB}} \simeq 10^{-8} \text{erg s}^{-1} \text{cm}^{-2} \text{sr}^{-1}$ to satisfy the CIB \times CXB correlation. From equations (1) and (17), the implied CXB flux is

$$F_{\text{CXB}} = 7 \times 10^{-13} \text{erg s}^{-1} \text{cm}^{-2} \text{deg}^{-2} \left(\frac{1.0}{\sqrt{\mathcal{C}}} \right) \left(\frac{0.1}{\Delta_{\text{cl}}} \right). \quad (18)$$

Since F_{CXB} is minimized for perfectly coherent sources, $\mathcal{C} = 1$, this value represents the amount of X-ray flux associated with the CIB sources whereas it is a lower limit for the total unresolved CXB. However, this flux can be accommodated by independent measurements of the unresolved CXB in (Hickox & Markevitch 2006) but is only marginally consistent with Moretti et al. (2012) who find only $\sim 3 \times 10^{-13} \text{erg s}^{-1} \text{cm}^{-2} \text{deg}^{-2}$ to be still unresolved.⁵ However, Moretti et al. (2012) do not include energies $< 1.5 \text{keV}$ in their fit for the CXB spectrum which could be the source of their lower derived 0.5–2 keV flux. On the other hand, the required F_{X} could itself be reduced if (i) the large-scale clustering of the underlying sources is stronger, say with $\Delta_{\text{cl}} \gtrsim 0.2$, or (ii) if the CIB \times CXB level at large scales is actually lower in reality, which is possible within the uncertainties, bringing it into agreement with low- z AGN and X-ray binaries (XRBS) (Helgason et al. 2014).

To illustrate these requirements, we display four simplistic SEDs in Fig. 10 where we assume an optical/UV component and an X-ray component that is a factor of $10^{-1}, 10^{-2}, 10^{-3}, 10^{-4}$ less energetic. We refer to these in terms of the X-ray to optical ratio, $X/O = -1, -2, -3$ and -4 , respectively, where $X/O = \log_{10} L_{\text{X}} / L_{\text{O}}$ with L_{X} and L_{O} integrated in the ranges $(1+z)[0.5, 2] \text{keV}$ and $[4.5/(1+z), 0.091] \mu\text{m}$, respectively, with $z = 10$. These ratios are already significantly lower than locally observed AGN which exhibit $X/O \sim 0$ on average but a suppressed X-ray component is

⁵ We have converted the 1.5 keV flux of Moretti et al. (2012) to 0.5–2 keV using their spectral index $\Gamma = 0.1$.

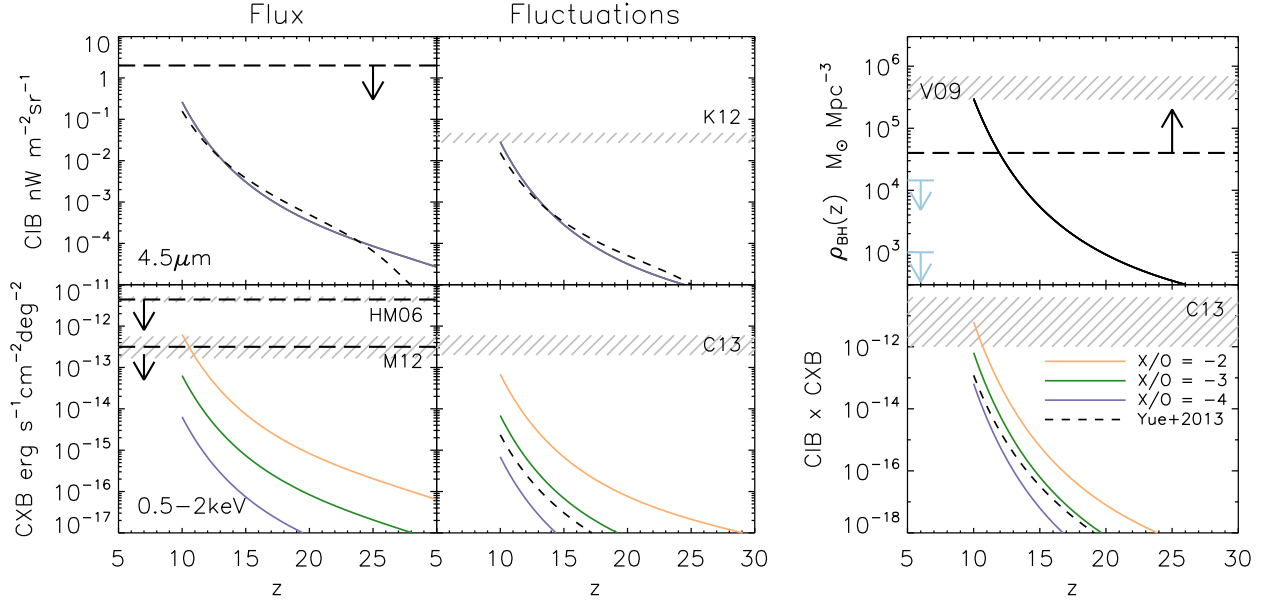


Figure 11. Left: the cumulative CIB (upper) and CXB (lower) from black holes at high- z growing according to the BH growth in the upper right panel. The ρ_{acc} at $z = 10$ has been chosen such that the measured $\delta F_{4.5\mu\text{m}} = 0.037 \pm 0.010$ is reproduced (marked as K12, Kashlinsky et al. 2012). The results here are mostly independent of the growth history and the individual BH masses. The upper left panel shows the resulting $F_{4.5\mu\text{m}}$ CIB where TeV upper limits from Meyer et al. (2012) are also shown. The lower panels show the CXB assuming three SED templates for the $X/O = -2, -3, -4$ (yellow, green, blue) and that from Yue et al. (2013b, dashed curve) shown in Fig. 10. Different upper limits for the CXB from Hickox & Markevitch (2006, HM06) and Moretti et al. (2012, M13, converted to 0.5–2 keV flux) are shown as dashed lines with 1σ uncertainties as grey regions. The levels of the large-scale CXB fluctuations are shown in the lower right panel with the measured levels of Cappelluti et al. (2013, C13) shown for reference. Right: accreted mass density in black holes growing at Eddington with $\epsilon = 0.1$ reaching $\rho_{\text{BH}} = 3 \times 10^5 M_{\odot} \text{Mpc}^{-3}$ by $z = 10$ (solid). The dashed line shows the lower limit for δF_{CIB} to be produced according equation (16) in the extreme limit $f_{\text{sed}} = 1$ and $\epsilon = 0.4$. The mass density locked in SMBHs at $z = 0$ is also shown for reference as grey regions (Vika et al. 2009, V09) and upper limits at $z \sim 6$ from Salvaterra et al. (2012) and Treister et al. (2013) in blue (upper and lower, respectively). The lower panel shows the CIB \times CXB fluctuations in units of $\text{erg s}^{-1} \text{cm}^{-2} \text{nW m}^{-2} \text{sr}^{-2}$. Notice how the $X/O = -2$ case (yellow) is the only one to reach the measured levels of Cappelluti et al. (2013) and Yue et al. (2013b, dashed) appears notably below this level.

possible for highly obscured BHs. The ionizing photons are then absorbed by the thick gas and reprocessed into nebular emission in the UV/optical ($\text{Ly } \alpha$, free-free), enhancing the CIB contribution (Yue et al. 2013b). In this way, a larger fraction f_{sed} of the bolometric luminosity ends up in the CIB, requiring less accretion on to BHs (see Fig. 9). We display the emerging SED from the highly obscured DCBH model of Yue et al. (2013b) in Fig. 10 for comparison. The energy at longer IR/radio wavelengths, and shorter γ -ray wavelengths are assumed to be negligible in comparison.

Fig. 11 shows the cumulative CIB and CXB flux including fluctuations and CIB \times CXB cross-fluctuations resulting from these broadband SEDs. Because the shape of the growth history does not matter much, we simply assume a scenario in which all BHs grow at the Eddington rate with $\epsilon = 0.1$, reaching a fixed accreted mass density at $z_{\text{end}} = 10$ ($\equiv \rho_{10}$)

$$\rho_{\text{acc}}(z) = \rho_{10} \exp \left[- \left(\frac{1 - \epsilon}{\epsilon} \right) \frac{t_{10} - t_z}{t_{\text{Edd}}} \right], \quad (19)$$

where $t_{\text{Edd}} \simeq 0.45$ Gyr is the Eddington time-scale. The results are also not sensitive to the choice of z_{end} as long as we keep ϵ and ρ_{10} fixed. We have chosen $\rho_{10} = 3 \times 10^5 M_{\odot} \text{Mpc}^{-3}$ such that the δF_{CIB} is reproduced. We find that the indicative large-scale CIB \times CXB signal can only be attained when $X/O \sim -2$. At the same time, the unresolved CXB implied by $X/O \gtrsim -2$ is in slight tension (1σ) with the most stringent limits measured by Moretti et al. (2012, see Fig. 11, bottom left). The spectrum of Yue et al. (2013b) having $-4 < X/O < -3$ is shown as a dashed line in Fig. 11, and appears notably below the CIB \times CXB requirement. This means that

the Yue et al. (2013b) model actually falls short of the X-ray energy implied by the coherent CXB levels but is nevertheless consistent with the CIB levels.

It is important to emphasize that the sources producing the CIB and CXB are not necessarily the same physical emitters and are in general a mixture of stars and BHs sharing the same large-scale structures. However, if they are predominantly BHs emitting in both optical and X-rays they will be accompanied by ionizing UV emission. For AGN spectra, this contribution is estimated by connecting the optical and X-ray part of the spectrum with a power-law slope, shown as dashed lines in Fig. 10. If we adopt the measured amplitudes of the CIB and CXB fluctuations we obtain a slope ranging from $\text{dlog}(F_{\text{O}}/F_{\text{X}})\text{dlog}E = -0.5$ to -0.7 and the resulting ionization rate exceeds the recombination rate in all cases such that $t_{\text{reion}} \ll t_{\text{recomb}}$. This means that in the presence of such production rate of ionizing photons at $z \gtrsim 10$, the Universe will reionize in the matter of \sim tens of Myr. For the CIB \times CXB signal to arise from the same type of sources therefore requires the suppression of UV photons escaping into the IGM ($f_{\text{esc}} < 1$), e.g. the BHs to be ultra-obscured (Ricotti, Ostriker & Gnedin 2005; Comastri et al. 2015). This would be easier with unconventional BHs such as DCBHs rather than X-ray binaries from stellar remnants which are much less obscured and are limited in growth by the mass and lifetime of the companion star (e.g. Yue et al. 2014; Tanaka & Li 2014; Pacucci & Ferrara 2015). Also, for an abundant population of small BHs, a proportionally greater fraction of the net mass goes into the seed of the gravitational collapse and does not contribute to ρ_{acc} .

5 SUMMARY AND DISCUSSION

In this paper, we assessed the possibility that the established clustering signal in the source-subtracted CIB fluctuations at near-IR originates in the early universe. We consider emission from star formation and BH accretion during the first 500 Myr and establish the physical requirements and consequences to reach the measured CIB values. Our results can be broadly summarized as follows:

(i) The contribution from high- z galaxies, with star formation efficiency set to $f_* = 0.005$ to match the LF from the deep *HST* Legacy surveys, cannot reproduce the levels of unresolved fluctuations in the near-IR for any reasonable extrapolation, producing merely $\sim 0.01\text{--}0.05 \text{ W m}^{-2} \text{ sr}^{-1}$ flux at $z > 8$. In fact, faint galaxies at intermediate- z make a larger contribution but are themselves insufficient to account for the entire clustering signal (Helgason et al. 2012). This conclusion is in agreement with previous studies (Fernandez et al. 2012; Cooray et al. 2012a; Yue et al. 2013a).

(ii) A simple extrapolation of the faint-end of the LF suggests that high- z galaxies will become significant once sources have been removed down to $m_{\text{AB}} \gtrsim 32$. Using the CIB to probe these populations will therefore require *JWST* (Kashlinsky et al. 2015) and/or cross-correlation techniques (Atrio-Barandela & Kashlinsky 2014).

(iii) For more energetically efficient modes of star formation, we find that heavier IMFs still require high star formation efficiencies $f_* > 0.1$ which must either take place in small haloes or end before $z \simeq 12$. The ionizing photons associated with such a population would have to be suppressed to avoid rapid reionization and to enhance the nebular emission contributing to the CIB. In other words, it would require very low escape fractions, $f_{\text{esc}} < 0.1$ per cent, in low-mass systems towards high redshifts (see also Fernandez et al. 2010). This is contrary to what is found in theoretical studies (Ferrara & Loeb 2013; Kuhlen & Faucher-Giguère 2012).

(iv) The cumulative CIB contribution of the fossils of the first galaxies that contain old stellar populations radiating throughout cosmic history is comparable to that of their high- z progenitors. Since many such systems will merge or become satellites of larger galaxies, their net contribution to the source-subtracted CIB is smaller and can be safely neglected as long as the contribution of the high- z counterparts is also low.

(v) For the CIB fluctuations to be produced by accreting BHs, one requires vigorous accretion rates in the early universe reaching $\rho_{\text{acc}} \gtrsim 10^5 \text{ M}_{\odot} \text{ Mpc}^{-3}$ by $z = 10$. This quantitative limit assumes a constant efficiency but is mostly independent of the accretion rate history and BH seed masses. The accretion must be very radiatively efficient at early times and then drop to inefficient growth throughout most of the remaining cosmic time with the resulting population largely unaccounted for in the SMBH census in local universe (Vika et al. 2009). In addition, this population must be extremely gas obscured in order to (i) avoid reionizing the universe too rapidly, (ii) to suppress the associated soft X-ray background and (iii) to enhance the fraction of energy emitted in the UV as reprocessed nebular emission. Yue et al. (2013b) have designed a novel model of DCBH formation that is broadly consistent with these requirements.

(vi) For the expected level of clustering of sources (both at low- and high- z), the minimum soft CXB flux implied by the measured CIB \times CXB cross-correlation, $F_X \simeq 7 \times 10^{-13} \text{ erg s}^{-1} \text{ cm}^{-2} \text{ deg}^{-2}$, is only marginally consistent with the most stringent CXB limits (Moretti et al. 2012). At face value this means that either (i) that high- z BHs require the entire available unresolved CXB, (ii) the clustering of the underlying sources is stronger (e.g. more biased) with $\Delta_{\text{cl}} \gtrsim 0.2$ at subdegree scales, or (iii) the high current uncertainty of the CIB \times CXB level at large scales could eventually

bring it into agreement with low- z AGN and XRBs (Helgason et al. 2014).

In this paper, we explored the physical requirements for stellar emission and accretion separately. It is however entirely possible, and in fact plausible, that the CIB and CXB are not produced by the same physical sources. The most intuitive scenario would have the CIB produced by stars, whereas accreting BHs sharing the same structures are responsible for the CIB \times CXB correlation. This would be a more natural way to obtain the $F_{\text{IR}}/F_X \sim 100$ ratio, which is unconventional for BHs only. The requirements for BHs to produce the CIB \times CXB component only, either stellar remnants or DCBHs, are much less energetically demanding than for the single-population explanation of the CIB and CIB \times CXB fluctuations. However, whereas rapid reionization is more easily avoided, one still requires the entire unresolved CXB available and is then left with the problem of explaining the CIB, the subject of this paper, by other means.

Our study of stellar sources isolates a narrow corner of parameters required for explaining the properties of the measured CIB fluctuations in terms of physics and evolution at high- z . The predominant contributions would then have to come from very massive stars ($\gtrsim 100 \text{ M}_{\odot}$), and accreting BHs, with non-instantaneous reionization in a highly clumped IGM. The area covered by this narrow corner may be widened by a factor of a few by relaxing assumptions of constancy of parameters such as f_* or ϵ . Apart from nucleosynthesis and accretion, an additional emission component at high- z may come from stellar collisions in the dense stellar system phase which may result from stellar dynamical evolution of the early systems (e.g. Kashlinsky & Rees 1983). The specific weight of this component is hard to quantify in a robust model-independent manner, but it may result in additional energy releases and ultimately formation of supermassive BHs (Begelman & Rees 1978). It is important to emphasize that narrow allowed parameter space is predicated on (1) the assumption of accurate estimate of the power contained in the primordial density spectrum at very small scales (comoving kpc), and (2) the assumption of its time invariance after the first sources form. The first drives the collapse of the first haloes with tiny modifications in the amount of power leading to exponentially different $f_{\text{col}}(z)$ and, consequently, different, potentially larger CIB. The second possibility may arise from the inevitable and highly complex interaction between the condition of the density field which forms early collapsing objects and the energy releasing sources (e.g. Ostriker & Cowie 1981; Rees 1985). We note that a possibly similar difficulty has been noted by Steinhart et al. (2015), concerning the hierarchical gravitation clustering prescription for formation of dark halos based on the predetermined Λ CDM power spectrum. If, empirically, the CIB fluctuations turn out to arise at early times, this may necessitate a modification in the adopted paradigm for object formation at $z \gtrsim 8\text{--}10$ (e.g. Hirano et al. 2015).

All this argues for empirically measuring the CIB fluctuations with required fidelity, establishing its nature and then constructing and identifying the implied physics models for the sources producing the signal with all its properties. This has been attempted in multi-wavelength cross-correlation studies that provide further constraints for theoretical models of both low- z and high- z sources as well as foreground emissions (e.g. Kashlinsky et al. 2007c, 2012; Cappelluti et al. 2013; Thacker et al. 2015). Additional information on the physics and evolution at early times would come by looking for correlations between the CIB and 21 cm maps (Fernandez et al. 2014; Mao 2014). *Euclid*'s large sky coverage and wavelengths make it particularly suitable for using its to-be-measured CIB

fluctuations to isolate emissions from the epoch of re-ionization (Kashlinsky et al. 2015) and identifying the condition of the IGM by cross-correlating *Euclid's* measured source-subtracted all-sky CIB and CMB maps (Atrio-Barandela & Kashlinsky 2014). A specific experiment has been recently proposed with the *JWST/NIRCAM* to probe the Lyman break of the CIB component and to tomographically reconstruct the emissions out to $z \gtrsim 30$ (Kashlinsky et al. 2015); the Lyman tomography method proposed there was shown to already lead to interesting limits at $z \gtrsim 30$ from the available *Spitzer* CIB maps at 3.6 and 4.5 μm . The nature of the CIB fluctuations should be resolvable in the coming decade and the emissions produced during the epoch of reionization identified from its properties, shedding light on the physics and evolution at that time.

ACKNOWLEDGEMENTS

We thank B. Yue, A. Ferrara, N. Cappelluti and E. Komatsu for useful discussions. KH was supported by the European Unions Seventh Framework Programme (FP7-PEOPLE-2013-IEF) under grant agreement number 628319-CIBorigins, and by NASA Headquarters under the NESSF Program Grant – NNX11AO05H. MR acknowledges support from NSF CDI-typeII grant CMM11125285 and the Theoretical and Computational Astrophysics Network (TCAN) grant AST1333514. AK acknowledges NASA's support for the *Euclid* LIBRAE project NNN12AA01C. VB was supported by NSF grant AST-1413501.

REFERENCES

- Ackermann M. et al., 2012, *Science*, 338, 1190
 Arendt R. G., Kashlinsky A., Moseley S. H., Mather J., 2010, *ApJS*, 186, 10
 Ashby M. L. N. et al., 2013, *ApJ*, 769, 80
 Atrio-Barandela F., Kashlinsky A., 2014, *ApJ*, 797, L26
 Barkat Z., Rakavy G., Sack N., 1967, *Phys. Rev. Lett.*, 18, 379
 Begeelman M. C., Rees M. J., 1978, *MNRAS*, 185, 847
 Behroozi P. S., Wechsler R. H., Conroy C., 2013, *ApJ*, 770, 57
 Bateau J., Williams D. A., 2015, *ApJ*, 812, 60
 Bouwens R. J., Illingworth G. D., Franx M., Ford H., 2007, *ApJ*, 670, 928
 Bouwens R. J. et al., 2015, *ApJ*, 803, 34
 Bovill M. S., Ricotti M., 2009, *ApJ*, 693, 1859
 Bovill M. S., Ricotti M., 2011a, *ApJ*, 741, 17
 Bovill M. S., Ricotti M., 2011b, *ApJ*, 741, 18
 Bromm V., 2013, *Rep. Prog. Phys.*, 76, 112901
 Cappelluti N. et al., 2013, *ApJ*, 769, 68
 Comastri A., Gilli R., Marconi A., Risaliti G., Salvati M., 2015, *A&A*, 574, L10
 Cooray A., Sheth R., 2002, *Phys. Rep.*, 372, 1
 Cooray A., Yoshida N., 2004, *MNRAS*, 351, L71
 Cooray A., Bock J. J., Keatin B., Lange A. E., Matsumoto T., 2004, *ApJ*, 606, 611
 Cooray A., Gong Y., Smidt J., Santos M. G., 2012a, *ApJ*, 756, 92
 Cooray A. et al., 2012b, *Nature*, 490, 514
 Dwek E., Arendt R. G., 1998, *ApJ*, 508, L9
 Eisenstein D. J., Hu W., 1998, *ApJ*, 496, 605
 Ellis R. S. et al., 2013, *ApJ*, 763, L7
 Fazio G. G. et al., 2004, *ApJS*, 154, 39
 Fernandez E. R., Komatsu E., 2006, *FrapJ*, 646, 703
 Fernandez E. R., Komatsu E., Iliev I. T., Shapiro P. R., 2010, *ApJ*, 710, 1089
 Fernandez E. R., Iliev I. T., Komatsu E., Shapiro P. R., 2012, *ApJ*, 750, 20
 Fernandez E. R., Zaroubi S., Iliev I. T., Mellema G., Jelić V., 2014, *MNRAS*, 440, 298
 Ferrara A., Loeb A., 2013, *MNRAS*, 431, 2826
 Finkelstein S. L. et al., 2015a, *ApJ*, 810, 71
 Finkelstein S. L. et al., 2015b, preprint ([arXiv:1504.00005](https://arxiv.org/abs/1504.00005))
 Furlanetto S. R., Loeb A., 2005, *ApJ*, 634, 1
 Greif T. H., Bromm V., 2006, *MNRAS*, 373, 128
 H. E. S. S. Collaboration. 2013, *A&A*, 550, A4
 Helgason K., Ricotti M., Kashlinsky A., 2012, *ApJ*, 752, 113
 Helgason K., Cappelluti N., Hasinger G., Kashlinsky A., Ricotti M., 2014, *ApJ*, 785, 38
 Hickox R. C., Markevitch M., 2006, *ApJ*, 645, 95
 Hinshaw G. et al., 2013, *ApJS*, 208, 19
 Hirano S., Zhu N., Yoshida N., Spergel D., Yorke H. W., 2015, preprint ([arXiv:1504.05186](https://arxiv.org/abs/1504.05186))
 Hummer D. G., 1994, *MNRAS*, 268, 109
 Iwamoto K. et al., 1998, *Nature*, 395, 672
 Jeon M., Pawlik A. H., Bromm V., Milosavljević M., 2014, *MNRAS*, 444, 3288
 Johnson J. L., Greif T. H., Bromm V., Klessen R. S., Ippolito J., 2009, *MNRAS*, 399, 37
 Kashlinsky A., 2005, *Phys. Rep.*, 409, 361
 Kashlinsky A., Rees M. J., 1983, *MNRAS*, 205, 955
 Kashlinsky A., Odenwald S., Mather J., Skrutskie M. F., Cutri R. M., 2002, *ApJ*, 579, L53
 Kashlinsky A., Arendt R., Gardner J. P., Mather J. C., Moseley S. H., 2004, *ApJ*, 608, 1
 Kashlinsky A., Arendt R. G., Mather J., Moseley S. H., 2005, *Nature*, 438, 45
 Kashlinsky A., Arendt R. G., Mather J., Moseley S. H., 2007a, *ApJ*, 654, L5
 Kashlinsky A., Arendt R. G., Mather J., Moseley S. H., 2007b, *ApJ*, 654, L1
 Kashlinsky A., Arendt R. G., Mather J., Moseley S. H., 2007c, *ApJ*, 666, L1
 Kashlinsky A., Arendt R. G., Ashby M. L. N., Fazio G. G., Mather J., Moseley S. H., 2012, *ApJ*, 753, 63
 Kashlinsky A., Mather J. C., Helgason K., Arendt R. G., Bromm V., Moseley S. H., 2015, *ApJ*, 804, 99
 Keenan R. C., Trouille L., Barger A. J., Cowie L. L., Wang W.-H., 2010, *ApJS*, 186, 94
 Kuhlén M., Faucher-Giguère C.-A., 2012, *MNRAS*, 423, 862
 Leitherer C. et al., 1999, *ApJS*, 123, 3
 Limber D. N., 1953, *ApJ*, 117, 134
 McLure R. J., Cirasuolo M., Dunlop J. S., Foucaud S., Almaini O., 2009, *MNRAS*, 395, 2196
 Madau P., Pozzetti L., 2000, *MNRAS*, 312, L9
 Madau P., Weisz D. R., Conroy C., 2014, *ApJ*, 790, L17
 Mao X.-C., 2014, *ApJ*, 790, 148
 Marconi A., Risaliti G., Gilli R., Hunt L. K., Maiolino R., Salvati M., 2004, *MNRAS*, 351, 169
 Matsumoto T. et al., 2005, *ApJ*, 626, 31
 Matsumoto T. et al., 2011, *ApJ*, 742, 124
 Matsumoto T., Kim M. G., Pyo J., Tsumura K., 2015, *ApJ*, 807, 57
 Mazin D., Raue M., 2007, *A&A*, 471, 439
 Meyer M., Raue M., Mazin D., Horns D., 2012, *A&A*, 542, A59
 Mitra S., Ferrara A., Choudhury T. R., 2013, *MNRAS*, 428, L1
 Moretti A., Vattakunnel S., Tozzi P., Salvaterra R., Severgnini P., Fugazza D., Haardt F., Gilli R., 2012, *A&A*, 548, A87
 O'Shea B. W., Wise J. H., Xu H., Norman M. L., 2015, *ApJ*, 807, L12
 Oke J. B., Gunn J. E., 1983, *ApJ*, 266, 713
 Ostriker J. P., Cowie L. L., 1981, *ApJ*, 243, L127
 Pacucci F., Ferrara A., 2015, *MNRAS*, 448, 104
 Pawlik A. H., Schaye J., Dalla Vecchia C., 2015, *MNRAS*, 451, 1586
 Planck Collaboration XVI et al., 2014, *A&A*, 571, A16
 Planck Collaboration XIII et al., 2015, preprint ([arXiv:1502.01589](https://arxiv.org/abs/1502.01589))
 Press W. H., Schechter P., 1974, *ApJ*, 187, 425
 Rees M. J., 1985, *MNRAS*, 213, 75P
 Ricotti M., Gnedin N. Y., 2005, *ApJ*, 629, 259
 Ricotti M., Shull J. M., 2000, *ApJ*, 542, 548
 Ricotti M., Gnedin N. Y., Shull J. M., 2002a, *ApJ*, 575, 33
 Ricotti M., Gnedin N. Y., Shull J. M., 2002b, *ApJ*, 575, 49
 Ricotti M., Ostriker J. P., Gnedin N. Y., 2005, *MNRAS*, 357, 207
 Ricotti M., Gnedin N. Y., Shull J. M., 2008, *ApJ*, 685, 21
 Robertson B. E., Ellis R. S., Furlanetto S. R., Dunlop J. S., 2015, *ApJ*, 802, L19

- Salvaterra R., Ferrara A., 2006, *MNRAS*, 367, L11
- Salvaterra R., Magliocchetti M., Ferrara A., Schneider R., 2006, *MNRAS*, 368, L6
- Salvaterra R., Haardt F., Volonteri M., Moretti A., 2012, *A&A*, 545, L6
- Santos M. R., Bromm V., Kamionkowski M., 2002, *MNRAS*, 336, 1082
- Schaerer D., 2002, *A&A*, 382, 28
- Seljak U., 2000, *MNRAS*, 318, 203
- Seo H. J., Lee H. M., Matsumoto T., Jeong W.-S., Lee M. G., Pyo J., 2015, *ApJ*, 807, 140
- Shankar F., Salucci P., Granato G. L., De Zotti G., Danese L., 2004, *MNRAS*, 354, 1020
- Sheth R. K., Mo H. J., Tormen G., 2001, *MNRAS*, 323, 1
- Soltan A., 1982, *MNRAS*, 200, 115
- Steinhardt C. L., Capak P., Masters D., Speagle J. S., 2015, preprint ([arXiv:1506.01377](https://arxiv.org/abs/1506.01377))
- Tanaka T. L., Li M., 2014, *MNRAS*, 439, 1092
- Tanaka T., Perna R., Haiman Z., 2012, *MNRAS*, 425, 2974
- Thacker C., Gong Y., Cooray A., De Bernardis F., Smidt J., Mitchell-Wynne K., 2015, *ApJ*, 811, 125
- Thompson R. I., Eisenstein D., Fan X., Rieke M., Kennicutt R. C., 2007a, *ApJ*, 657, 669
- Thompson R. I., Eisenstein D., Fan X., Rieke M., Kennicutt R. C., 2007b, *ApJ*, 666, 658
- Tinker J., Kravtsov A. V., Klypin A., Abazajian K., Warren M., Yepes G., Gottlöber S., Holz D. E., 2008, *ApJ*, 688, 709
- Treister E., Schawinski K., Volonteri M., Natarajan P., 2013, *ApJ*, 778, 130
- Tsumura K., Matsumoto T., Matsuura S., Sakon I., Wada T., 2013, *PASJ*, 65, 121
- Vika M., Driver S. P., Graham A. W., Liske J., 2009, *MNRAS*, 400, 1451
- Volonteri M., Bellovary J., 2012, *Rep. Prog. Phys.*, 75, 124901
- Weisz D. R., Dolphin A. E., Skillman E. D., Holtzman J., Gilbert K. M., Dalcanton J. J., Williams B. F., 2014, *ApJ*, 789, 148
- Yue B., Ferrara A., Salvaterra R., Chen X., 2013a, *MNRAS*, 431, 383
- Yue B., Ferrara A., Salvaterra R., Xu Y., Chen X., 2013b, *MNRAS*, 433, 1556
- Yue B., Ferrara A., Salvaterra R., Xu Y., Chen X., 2014, *MNRAS*, 440, 1263
- Zackrisson E., Rydberg C.-E., Schaerer D., Östlin G., Tuli M., 2011, *ApJ*, 740, 13
- Zemcov M. et al., 2014, *Science*, 346, 732

This paper has been typeset from a $\text{\TeX}/\text{\LaTeX}$ file prepared by the author.